INTERFEROMETRIC SAR MODELING OF GEOPHYSICS MEASUREMENTS

Andon Lazarov[1], Marat Grigoryan[2], Dimitar Minchev[3], Chavdar Minchev[4], Atanas Dimitrov[3]

[1]BFU, Burgas/K.N. Toosi University, [2]YSU, Yerevan, [3]BFU, Burgas, [4]Shumen University

Abstract: The geometry and basic parameters of Interferometric Synthetic Aperture Radar (InSAR) geophysics system are addressed In the present work. Equations of pixel height and displacement evaluation are derived. Interferogram and differential interferogram are generated based on a surface model and SAR measurements. Results of numerical experiments are provided.

1. Introduction - principles of SAR interferometry

Synthetic Aperture Radar (SAR) is a coherent microwave imaging system able to provide data all weather, day and night, guaranteeing global coverage. SAR interferometry is based on processing two or more complex valued SAR images obtained from different SAR positions [1-4]. InSAR is of geophysical meaning in topography evaluation of slopes, surface deformations (volcanoes, earthquakes, ice fields), glacier studies, vegetation growth, etc. The estimation of topographic height with essential accuracy is performed by the interferometric distance difference measured based on two SAR echoes from the same surface. Changes in topography (displacement), precise to a fraction of a radar wavelength, can be evaluated by differential interferogram generated by three or more successive complex SAR images [5, 6]. The main goal of the work is to describe multi pass In-SAR geometry and derive mathematical expressions for current distances between SAR's positions and individual pixels, and principal InSAR parameters: topographic height, and topographic displacement. The rest of the paper is organized as follow. InSAR geometry and kinematics is analytically described in section 2, 3-D. Equations of relief measurements are derived in section 3. Equations of relief displacement are provided in section 4. Modeling of SAR interferogram generation based on distance measurements is discussed in section 5. Results of numerical experiment are presented in section 6. Conclusion remarks are made in section 7.

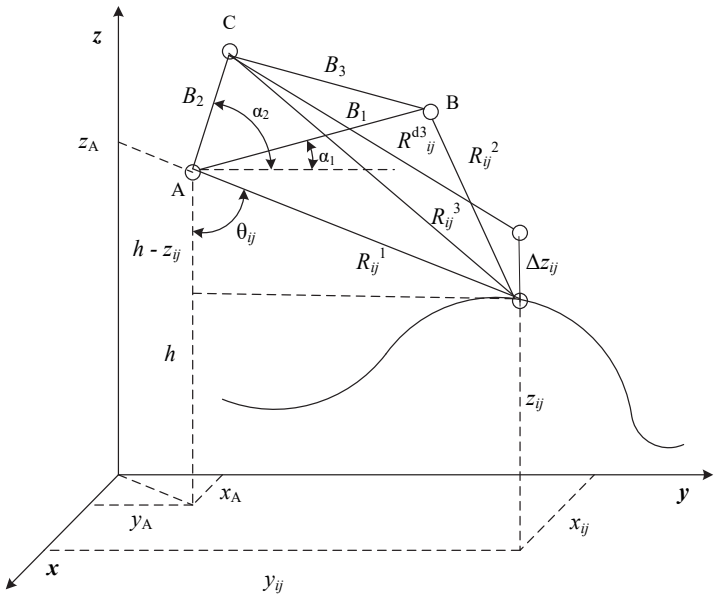

Fig. 1. Interferometric SAR geometry

2. InSAR geometry and kinematics

Assume a three-pass SAR system viewing three-dimensional (3-D) surface presented by discrete resolution elements, pixels. Each pixel is defined by the third coordinate $z_{ij}(x_{ij},y_{ij})$ in 3-D coordinate system $Oxyz$. Let A, B, and C, are SAR positions of imaging (Fig. 1). Between every SAR, $C_3^2 = 3$ In-SAR baselines can be drawn. The main geometric SAR characteristic is the time dependent distance vector from the SAR system at the *n*-th pass in the *p*-th moment to each pixel of the surface, defined in the coordinate system $Oxyz$, i.e.

$$\mathbf{R}_{ij}^{n}(p) = \mathbf{R}^{n}(p) - \mathbf{R}_{ij}, \tag{1}$$

where $n = 1 \div 3$ is the number of SAR passes, and $\mathbf{R}^{n}(p) = \mathbf{R}^{0n} + \mathbf{V}.p.T_p$ is the distance vector at the *n*-th SAR pass in the *p*-th moment, $\mathbf{R}^{0n}$ is the initial distance vector at the *n*-th SAR pass, $\mathbf{R}_{ij}$ is the distance vector of the ij - th pixel.

3. InSAR relief measurements

The distances to ij -th pixel from SAR at *m*-th and *n*-th pass ($m \neq n$) in the moment of imaging can be defined by the cosines theorem, i.e.

$$\left|\mathbf{R}_{ij}^{n}\right| = \left\{\left|\mathbf{R}_{ij}^{m}\right|^2 + B_{mn}^2 - 2B_{mn}\left|\mathbf{R}_{ij}^{m}\right|\cos\left[\frac{\pi}{2} - [\theta^{m}{}_{ij} - \alpha_{mn})]\right]\right\}^{\frac{1}{2}}, \tag{2}$$

where B_{mn} is the modulus of the baseline vector, $\theta^{m}{}_{ij}$ is the look angle, α_{mn} is a priory known tilt angle, the angle between baseline vector and plane *Oxy*. The look angle $\theta^{m}{}_{ij}$ and height z_{ij} of the *ij*-th pixel on the surface with respect to the *m*-th SAR position in the moment of imaging can be written as

$$\theta^m{}_{ij} = \alpha_{mn} + \arcsin\frac{\left|\mathbf{R}_{ij}^m\right|^2 + B_{mn}^2 - \left|\mathbf{R}_{ij}^n\right|^2}{2B_{mn}\left|\mathbf{R}_{ij}^m\right|}, \quad (3)$$

$$z_{ij} = h^m - \left|\mathbf{R}_{ij}^m\right|\cos\theta^m{}_{ij}. \quad (4)$$

The distance difference $\left|\Delta\mathbf{R}_{ij}^{mn}\right| = \left|\mathbf{R}_{ij}^n\right| - \left|\mathbf{R}_{ij}^m\right|$, can be expressed by an interferometric phase difference $\left|\Delta\mathbf{R}_{ij}^{mn}\right| = \frac{\lambda}{2\pi}\Delta\varphi_{ij}^{mn}$. In case $\left|\mathbf{R}_{ij}^m\right|$ can be measured, i.e. $\left|\mathbf{R}_{ij}^n\right| = \left|\mathbf{R}_{ij}^m\right| + \left|\Delta\mathbf{R}_{ij}^{mn}\right|$, then

$$\theta^m{}_{ij} = \alpha_{mn} + \arcsin\left[\frac{B_{mn}}{2R_{ij}^m} - \frac{\lambda}{2\pi B_{mn}}\Delta\varphi_{ij}^{mn}\left(1 + \frac{\lambda}{4\pi R_{ij}^m}\Delta\varphi_{ij}^{mn}\right)\right] \quad (5)$$

$$z_{ij} = h^m - R_{ij}^m.\cos\left\{\alpha_{mn} + \arcsin\left[\frac{B_{mn}}{2R_{ij}^m} - \frac{\lambda}{2\pi B_{mn}}\Delta\varphi_{ij}^{mn}.\left(1 + \frac{\lambda}{4\pi R_{ij}^m}\Delta\varphi_{ij}^{mn}\right)\right]\right\} \quad (6)$$

4. InSAR measurements of relief displacement

Consider a three pass SAR interferometry (Fig. 1). Let A and B be the two positions of imaging which can be defined by two passes of the same spaceborne SAR in different time (two pass interferometry). The third position C is defined by third pass of the spaceborne SAR. The surface displacement Δz_{ij}, due to, for instance, an earthquake could derive from two SAR interferograms built before and after the seismic impact. The temporal baseline, the time scale over which the displacement is measured, must be following the dynamics of the geophysical phenomenon. Short time baseline is applied for monitoring fast surface changes. Long temporal baseline is used for monitoring slow geophysics phenomena (subsidence). The interferometry phase before event is derived from complex images acquired by A and B SAR positions in the moment of imaging, while the interferometry phase after event is derived from complex images acquired by A and C SAR positions in the moment of imaging. The distances R_{ij}^1, R_{ij}^2, R_{ij}^3 and R_{ij}^{d3} after standard manipulations are written as [7]

$$R_{ij}^2 \cong R_{ij}^1 - B_1\sin(\theta_{ij} - \alpha_1) + \frac{B_1^2}{2R_{ij}^1}, \quad R_{ij}^3 \cong R_{ij}^1 - B_2\sin(\theta_{ij} - \alpha_2) + \frac{B_2^2}{2R_{ij}^1}$$

$$R_{ij}^{d3} \cong R_{ij}^3 - \Delta z\left(\cos\theta_{ij} + \frac{B_2}{R_{ij}^1}\sin\alpha_2\right) + \frac{(\Delta z_{ij})^2}{2R_{ij}^1}, \quad (7)$$

where R_{ij}^1, R_{ij}^2 and R_{ij}^3 are the slant ranges from A, B and C positions of SAR system to the observed pixel in the moment of imaging before the surface displacement and R_{ij}^{d3} are the slant range from C SAR position to the observed pixel after Δz_{ij} surface displacement.

Given SAR wavelength λ, the phase differences proportional to range differences related to a particular pixel before and after displacement in the moment of imaging can be written as

$$\varphi^{\mathrm{AB}} = \frac{4\pi}{\lambda}(R_{ij}^1 - R_{ij}^2), \quad \varphi^{\mathrm{AC}} = \frac{4\pi}{\lambda}(R_{ij}^1 - R_{ij}^3), \quad \varphi_{\mathrm{d}}^{\mathrm{AC}} = \frac{4\pi}{\lambda}(R_{ij}^1 - R_{ij}^{\mathrm{d}3}) \tag{8}$$

Neglecting the term $(\Delta z)^2 / 2R_{ij}^1$ in (7), (8) can be rewritten as

$$\varphi^{\mathrm{AB}} = \frac{4\pi}{\lambda}\left(B_1 \sin(\theta_{ij} - \alpha_1) - \frac{B_1^2}{2R_{ij}^1}\right), \quad \varphi^{\mathrm{AC}} = \frac{4\pi}{\lambda}\left(B_2 \sin(\theta_{ij} - \alpha_2) - \frac{B_2^2}{2R_{ij}^1}\right);$$

$$\varphi_{\mathrm{d}}^{\mathrm{AC}} = \frac{4\pi}{\lambda}\left[B_2 \sin(\theta_{ij} - \alpha_2) - \frac{B_2^2}{2R_{ij}^1} + \Delta z\left(\cos\theta_{ij} + \frac{B_2}{R_{ij}^1}\sin\alpha_2\right)\right]; \tag{8}$$

$$= \varphi^{\mathrm{AC}} + \Delta z\left(\cos\theta_{ij} + \frac{B_2}{R_{ij}^1}\sin\alpha_2\right) \tag{9}$$

The displacement Δz_{ij} is extracted from the differential interferometric phase difference $\Delta\Phi_{\mathrm{d}} = \varphi_{\mathrm{d}}^{\mathrm{AC}} - \varphi^{\mathrm{AB}}$. Considering $B_2 / R_{ij}^1 << 1$, then $\Delta\Phi_{\mathrm{d}} = \Delta\Phi + \frac{4\pi}{\lambda}\Delta z_{ij}\cos\theta_{ij}$, where

$$\Delta\Phi = \frac{4\pi}{\lambda}\left[B_2 \sin(\theta_{ij} - \alpha_2) - B_1 \sin(\theta_{ij} - \alpha_1) - \frac{B_2^2 - B_1^2}{2R_{ij}^1}\right]. \tag{10}$$

For surface displacement z_{ij} can be written

$$\Delta z_{ij} = \frac{\lambda}{4\pi}\frac{\Delta\Phi_{\mathrm{d}} - \Delta\Phi}{\cos\theta_{ij}}. \tag{11}$$

5. InSAR modeling of geophysical measurements

Consider 3-pass InSAR geometry (Fig.1). The vector distances from the SAR positions to each ij -th pixel from the region of interest are $\mathbf{R}_{ij}^{\mathrm{S}} = \mathbf{R}^{\mathrm{S}} - \mathbf{R}_{ij}$, where $\mathrm{S} = \mathrm{A}, \mathrm{B}, C$ denotes the SAR position in the moment of imaging, $\mathbf{R}^{\mathrm{S}} = [x_{\mathrm{S}}, y_{\mathrm{S}}, z_{\mathrm{S}}]^T$ denotes the SAR vector position, $\mathbf{R}_{ij} = [x_{ij}, y_{ij}, z_{ij}]^T$ denotes the ij -th pixel vector position. Coordinates of SAR positions in the

moment of imaging are as follows: for a master SAR position A, x_{A}, y_{A}, z_{A}; for a slave SAR position B, x_{B}, y_{B}, z_{B}; for a slave SAR position C, x_{C}, y_{C}, z_{C}.

After distance measurements from the master SAR position A and slave SAR positions B and C, respectively to each ij -th pixel on the surface, and co-registration of so obtained master image and slave images the instrumental interferometric phase differences are calculated by

$$\varphi_{ij}^{\mathrm{AB}} = \frac{4\pi}{\lambda}\left(\left|\mathbf{R}_{ij}^{\mathrm{A}}\right| - \left|\mathbf{R}_{ij}^{\mathrm{B}}\right|\right) - 2\pi.\max\left\lceil\frac{2}{\lambda}\left(\left|\mathbf{R}_{ij}^{\mathrm{A}}\right| - \left|\mathbf{R}_{ij}^{\mathrm{B}}\right|\right)\right\rceil,$$

$$\varphi_{ij}^{\mathrm{AC}} = \frac{4\pi}{\lambda}\left(\left|\mathbf{R}_{ij}^{\mathrm{A}}\right| - \left|\mathbf{R}_{ij}^{\mathrm{C}}\right|\right) - 2\pi.\max\left\lceil\frac{2}{\lambda}\left(\left|\mathbf{R}_{ij}^{\mathrm{A}}\right| - \left|\mathbf{R}_{ij}^{\mathrm{C}}\right|\right)\right\rceil$$ - without pixel displacement,

$$\varphi_{ij,\mathrm{d}}^{\mathrm{AC}} = \frac{4\pi}{\lambda}\left(\left|\mathbf{R}_{ij}^{\mathrm{A}}\right| - \left|\mathbf{R}_{ij,\mathrm{d}}^{\mathrm{C}}\right|\right) - 2\pi.\max\left\lceil\frac{2}{\lambda}\left(\left|\mathbf{R}_{ij}^{\mathrm{A}}\right| - \left|\mathbf{R}_{ij,\mathrm{d}}^{\mathrm{C}}\right|\right)\right\rceil$$ - with pixel displacement.

In order to unwrap the interferometric phases standard algorithms Matlab *unwrap* function, 2-D Costantini phase unwrapping based on network programming, and 2D Goldstein branch cut phase unwrapping, can be applied.

6. Numerical experiments

Consider a geo-tiff file of Dilijan region in Caucasusn, Armenia, located at the geographical coordinates: 40° 44' 27" north and 44° 51' 47" east longitude. Consider 2-pass InSAR scenario. Coordinates of SAR positions in the moment of imaging: master SAR position A, $x_{\mathrm{A}} = 0$ m, $y_{\mathrm{A}} = 3003\times10^{3}$ m, $z_{\mathrm{A}} = 3\times10^{5}$ m, slave SAR position B $x_{\mathrm{B}} = 0$ m, $y_{\mathrm{B}} = 300\times10^{3}$ m, $z_{\mathrm{B}} = 3\times10^{5}$ m. Wavelength is 0.05 m. Calculated distances from SAR position A and SAR position B to each pixel on the surface are illustrated in Fig. 2, (*a*), (*b*). interferogram wrapped phases (*c*) and unwrapped phases (*d*) are presented in Fig. 2, (*c*), (*d*).

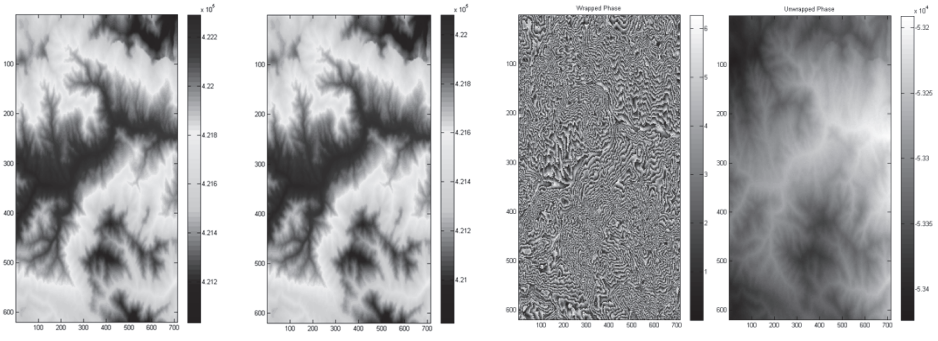

(*a*) (*b*) (*c*) (*d*)

Fig.2. Distances from SAR position A (*a*) and SAR position B (*b*) to each pixel on the surface in pseudo color map, interferogram wrapped phases (*c*) and unwrapped phases (*d*)

Consider 3-pass interferometric SAR scenario. and a surface before (Fig. 3, *a*) and after (Fig. 3, *b*) displacement described by Matlab function *peaks*. Coordinates of SAR positions in the moment of imaging: master SAR position A, $x_{\mathrm{A}} = 350$ km, $y_{\mathrm{A}} = 350$ km, $z_{\mathrm{A}} = 800$ km,

slave SAR position B $x_B = 351.5$ km, $y_B = 350$ km, $z_B = 800$ km., slave SAR position C $x_C = 350$ km, $y_C = 3512$ km, $z_C = 800$ m. Wavelength is 0.03 m.

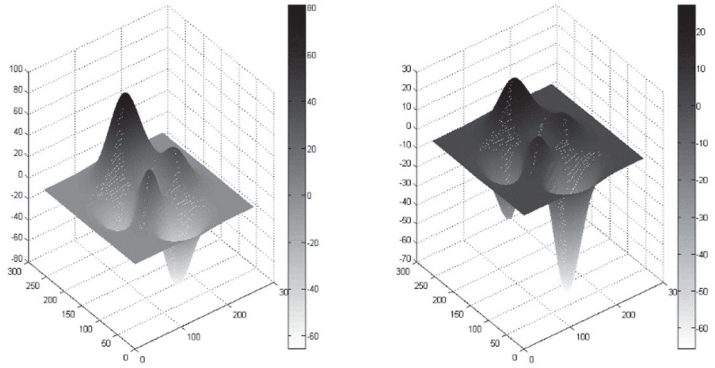

(*a*) (*b*)

Fig. 3. Surface (*peaks*) before (*a*), and after (*b*) displacement

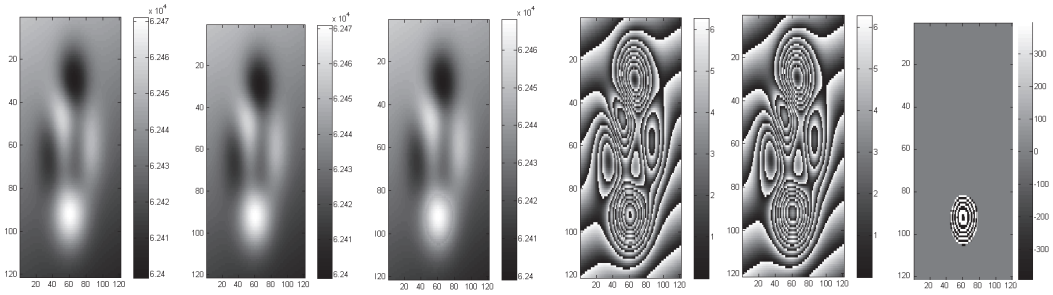

(*a*) (*b*) (*c*) (*d*) (*e*) (*g*)

Fig.4. Distances to the surface measured from SAR positions A (*a*), B (*b*), and C (*c*). AB interferogram (*d*), AC interferogram (*e*) with surface displacement, and differential interferogram AB-AC (*g*)

7. Conclusions

In the present work an InSAR approach has been suggested to model processes of interferograms and differential interferograms generation using geo-tiff files and measurements of distances from SAR positions to each pixels of the observed surface in the moment of imaging. Analytical expressions to calculate pixel heights and pixel displacement have been derived. Based on vector description of the InSAR scenario, interferometric and differential phase differences have been defined. This approach has been illustrated by results of numerical experiments.

REFERENCES

1. Pepe A., Calò F. A Review of Interferometric Synthetic Aperture RADAR (InSAR) Multi-Track Approaches for the Retrieval of Earth's Surface Displacements, Appl. Sci. 2017, 7, 1264; doi:10.3390/app7121264.
2. Pepe, A.; Bonano, M.; Zhao, Q.; Yang, T.; Wang, H. The Use of C-/X-Band Time-Gapped SAR Data and Geotechnical Models for the Study of Shanghai's Ocean-Reclaimed Lands through the SBAS-DInSAR Technique. Remote Sens. 2016, 8, 911
3. Hu, J., Ding, X., Li, Z., et al. Kalman-filterbased approach for multi-sensor, multitrack and multitemporal InSAR. IEEE Trans. Geosci. Remote Sens. 2013, 51, pp. 4226–4239.
4. Casu,F.;Manconi,A.;Pepe,A.;Lanari,R. Deformation time-series generation in areas characterized by large displacement dynamics: The SAR amplitude pixel-offset SBAS technique. IEEE Trans. Geosci. Remote Sens. 2011, 49, pp. 2752–2763.

5. Samsonov, S.; d'Oreye, N. Multidimensional time-series analysis of ground deformation from multiple InSAR data sets applied to Virunga Volcanic Province. Geophys. J. Int. 2012, 191, pp. 1095–1108.
6. Sansosti, E., Berardino, P., et al. How new generation SAR systems are impacting the analysis of ground deformation. Int. J. Appl. Earth Obs. Geoinf. 2014, 28, pp. 1–11.
7. Vettore, A., Ponte, S., et al. Space-based surface change detection with differential Synthetic Aperture Radar (SAR) Interferometry: potentialities and preliminary investigations. Symposium on Geospatial Theory, Processing and Applications, Ottawa, 2002.